Near-edge ligand stripping and robust radiative exciton recombination in CdSe/CdS Core/Crown nanoplatelets

Near-Edge Ligand Stripping and Robust Radiative Exciton Recombination in CdSe/CdS Core/Crown Nanoplatelets

Jari Leemans,[†,‡] Shalini Singh,[†,‡] Chen Li,[¶] Stephanie Ten Brinck,[§] Sara Bals,[¶] Ivan Infante,[‖] Iwan Moreels,[†,‡] and Zeger Hens[*,†,‡]

†*Physics and Chemistry of Nanostructures, Ghent University, 9000-Ghent, Belgium*

‡*Center for Nano and Biophotonics, Ghent University, 9000-Ghent, Belgium*

¶*Electron Microscopy for Materials Research (EMAT), University of Antwerp, Groenenborgerlaan 171, 2020 Antwerp, Belgium*

§*Department of Theoretical Chemistry, Faculty of Science, Vrije Universiteit Amsterdam, de Boelelaan 1083, 1081 HV Amsterdam, The Netherlands*

‖*Department of Nanochemistry, Istituto Italiano di Tecnologia, Via Morego 30, 16163 Genova, Italy*

E-mail: zeger.hens@ugent.be

Abstract

Colloidal nanocrystals are characterized by a strong relation between surface chemistry and opto-electronic properties, a point that is best elucidated by well-defined model systems. Here, we present a study on core/crown CdSe/CdS nanoplatelets (NPLs) synthesized with an atomically precise thickness and terminated by cadmium oleate ($Cd(Ol)_2$) covered (100) facets. While such CdSe/CdS NPL ensembles can have a photoluminescence quantum yield of 92%, transmission electron microscopy imaging still gives evidence of sample heterogeneity, where CdSe core NPLs are either decorated with complete or partial CdS crowns. Using solution nuclear magnetic resonance spectroscopy, we show that addition of butylamine to a NPL dispersion displaces up to $\sim$ 40% of the surface-bound $Cd(Ol)_2$. Opposite from CdSe core NPLs, dispersions of CdSe/CdS core crown NPLs with such incomplete ligand coverage can retain up to 45% of their initial photoluminescence efficiency. Moreover, the luminescent decay of such dispersions remains dominated by radiative exciton recombination. By means of density functional theory simulations, we argue that butylamine preferentially displaces $Cd(Ol)_2$ bound to (near)-edge surface sites. Accordingly, we assign the persistent radiative exciton recombination to the fraction of NPLs having a complete CdS crown, which prevents near-edge surface sites from trapping the exciton in the CdSe core. We conclude from these observations that Z-type ligands such as cadmium carboxylates provide sufficient electronic passivation of plain (100) facets, yet are prone to displacement from (near)-edge surface sites. This point highlights that strategies aimed at separating charge carriers from (near)-edge sites – such as crown growth rather than full shelling – can suffice to obtain colloidal semiconductor nanocrystals with a highly efficient and robust photoluminescence.

Graphical TOC Entry

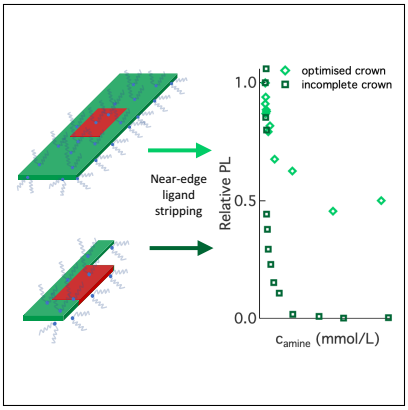

Keywords

2D Materials, Semiconductors, Colloidal Nanocrystals, Surface Chemistry, Nuclear Magnetic Resonance Spectroscopy, Trap States

Colloidal semiconductor nanocrystals (NCs) are a new class of opto-electronic materials that offer a combination of size-tunable optical properties and a suitability for solution-based processing.[1,2] NC research involves parallel efforts to establish new and improved synthesis protocols, understand light-matter interaction and explore the use of NCs in, for example, solar energy conversion, photodetection, and lighting and displays.[3–5] Applications such as lighting and displays typically rely on luminescent color conversion, for which the stability and efficiency of the NC photoluminescence is key.[6] From this perspective, the high fraction of surface atoms in NCs is a drawback.[7,8] Undercoordinated surface atoms can have dangling bonds that lead to localized electronic states within the band gap, thereby providing efficient pathways for non-radiative recombination of electron-hole pairs. Established strategies to avoid the formation of such trap states include the chemisorption of molecular ligands[9–13] and the epitaxial overgrowth of an original core NC with a shell made of a wide bandgap semiconductor.[14–17] Both approaches rely on the chemical passivation of undercoordinated surface atoms, an often made point that was recently confirmed in the case of CdSe NCs by theoretical studies on realistic model systems.[18,19] Here, it was found that in particular the desorption of Cd salts as Z-type ligands from the CdSe surface can leave behind di-coordinated surface Se atoms, which induce a localized, mid-gap state. The recent confirmation that saturating the NC surface with Z-type ligands can effectively lead to near unity photoluminescence quantum yields (PLQY) further highlights the underlying relation between the surface termination and the photoluminescence efficiency of NCs.[10,20]

Colloidal nanoplatelets (NPLs) are a unique class of NCs. Especially in the case of cadmium chalcogenides, NPLs with the zinc blende structure can be obtained as atomically flat, two-dimensional NCs featuring exactly the same atomically precise layer thickness across the entire ensemble.[21–27] Since the NPL thickness determines the exciton energy, macroscopic ensembles of CdSe NPLs are characterized by a spectrally narrow photoluminescence,[28] which can have a PLQY of 50%. Moreover, synthesis methods have been developed for the formation of heterostructures, which exhibit even higher PLQYs.[29–34]

Here, a second material is epitaxially grown as a shell that encompasses the initial core in a layered stack or as a crown that gives a lateral extension to the initial core. Not unlike quasi-spherical CdSe NCs, as-synthesized NPLs have top and side surfaces terminated by Cd salts, which upon removal lead to the formation of localized trap states.[35] Opposite from quasi-spherical NCs, however, NPLs have a well-defined crystallography with top and side surfaces consisting of (100) facets.[36] This makes them unique model systems to test surface chemistry/photoluminescence efficiency relations, where a recent experimental and theoretical study on ligand stripping suggests that the weakest binding sites for Cd salts are found near the NPL edges.[35] If correct, one would expect that a mere edge passivation suffices to form CdSe-based NPLs with a highly efficient and stable photoluminescence.

In this work, we address the conjecture that Cd salts most easily desorb from edge or near-edge adsorption sites by analyzing the stripping of cadmium oleate from CdSe/CdS core/crown heteronanoplatelets. Using scanning transmission electron microscopy (STEM) imaging in combination with elemental analysis, we confirm that CdS crown growth leads in most cases to the lateral extension of CdSe core NPLs by CdS. Similar to CdSe NPLs, we introduce a purification method that results in CdSe/CdS core/crown NPLs capped almost exclusively by cadmium oleate ($Cd(Ol)_2$) as Z-type ligands. By means of nuclear magnetic resonance (NMR) spectroscopy, we demonstrate that butylamine ($BuNH_2$) strips $Cd(Ol)_2$ from the core/crown surface, in line with the displacement of Z-type ligands by Lewis bases as described previously in the literature.[35,37,38] Not unlike CdSe NPLs, $BuNH_2$ only strips a part of the $Cd(Ol)_2$ terminating the CdSe/CdS core/crown NPLs. Moreover, we show that an ensemble of CdSe/CdS core/crown NPLs can preserve up to 45% of its initial PLQY even at $BuNH_2$ concentrations where 40% of the cadmium oleate initially present has been displaced. In addition, we find that the rate of radiative exciton recombination still dominates the luminescent decay of such an ensemble of stripped NPLs. By means of density functional theory (DFT) calculations for CdS NPLs, we argue that these observations reflect the preferential displacement of $Cd(Ol)_2$ from (near)-edge binding sites, which exhibit significantly

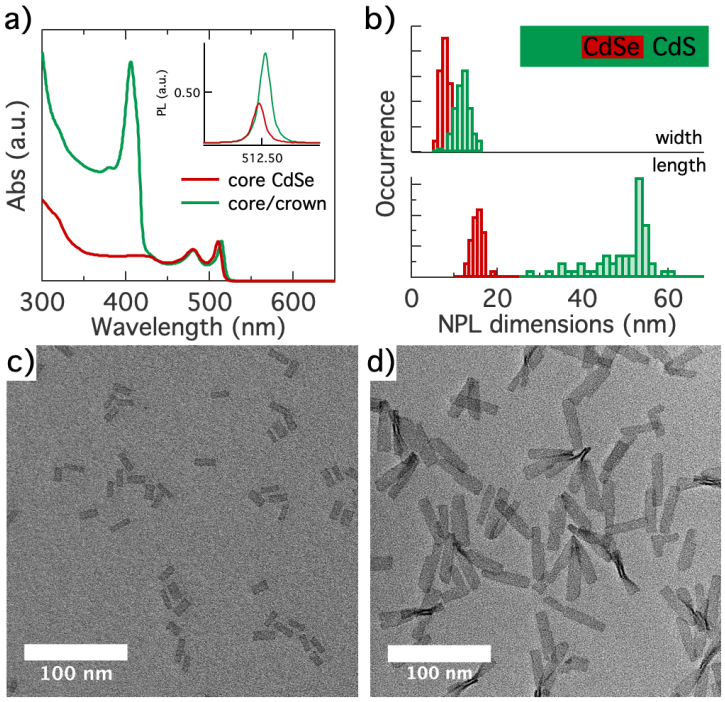

Figure 1: (a) Absorption spectrum of initial CdSe core and final CdSe/CdS core/crown nanoplatelets, normalised at the maximum of the heavy hole absorption line. Inset: photoluminescence spectra of core and core/crown nanoplatelets, with the surface area normalised to the respective PLQY. (b) Histograms of (top) width and (bottom) length of (red) the initial core and (green) the final core/crown nanoplatelets. Inset: scheme representing the average heterostructure to scale. (c) Overview bright-field TEM image of initial CdSe crown nanoplatelets. (d) The same for the final CdSe/CdS core/crown nanoplatelets.

weaker binding energies than sites in the center of a facet. Under such conditions, the localized trap states created by $Cd(Ol)_2$ displacement will not affect the PLQY nor the radiative recombination rate of CdSe/CdS core/crown NPLs with a sufficiently thick and homogeneous CdS crown. We thus conclude that protecting vulnerable edge sites is imperative to create colloidal semiconductor nanocrystals with an efficient and robust photoluminescence, a point that is well exemplified by the effects of CdS crown growth around core CdSe NPLs.

Core/crown CdSe/CdS NPLs were synthesised by means of a continuous injection approach, similar to what was reported in the literature.[33,34] As described in detail in Supporting Information S1, 4.5 ML CdSe NPLs were first prepared and purified according to known methods.[25] Next, these core NPLs were dispersed in 1-octadecene (ODE) together

with Cd-acetate. After heating this mixture to 200°C under inert atmosphere, a transparent solution of Cd-octanoate and elemental S was slowly added at a rate of 15 mL/hour to grow the CdS crown. The absorption spectra of the thus obtained core and core/crown NPLs are represented in Figure 1a. Most importantly, the absorption spectrum of the core/crown NPLs features both the absorption lines of the heavy and light-hole exciton of 4.5 ML CdSe NPLs at 514 nm and 480 nm and the exciton line at 406 nm that is characteristic of 4.5 ML CdS NPLs. On the other hand, the PL spectrum of CdSe/CdS NPLs recorded after photo-excitation at 370 nm only exhibits a slightly red-shifted emission from CdSe excitons, not from CdS excitons, see inset of Figure 1a and Supporting Information S2. Finally, using the crown growth as described in Supporting Information S1, CdS growth increases the PLQY of the initial CdSe NPLs from 40% to 92%. Rather than a separate mixture of CdSe and CdS NPLs, these results point towards the formation of core/crown structures in which excitons formed in the CdS crown are rapidly transferred to the CdSe core, and where the CdS crown effectively passivates the remaining trap states at the CdSe NPL surface.

We evaluated the sizes as well as the morphology of the core-only and core/crown NPLs by means of bright-field transmission electron microscopy (TEM) images. Starting from the NPL projections in TEM images, we determined the distribution of the length and width for core and core/crown NPLs. As can be seen in Figure 1b, crown growth extends the length and width of the average NPL from 15.0×6.5 nm to 48.5×10.1 nm, suggesting that each CdSe edge is covered by 1.8 nm (long edges) to 9.8 nm (short edges) of CdS on average. The top view projection of multiple core/crown NPLs in Figure 1d indicates that the rectangular shape of the initial core NPLs in Figure 1c is largely conserved upon crown growth. We found that using rather small core CdSe NPLs as initial seeds, Cd-octanoate as the precursor for CdS overgrowth, and rather high addition rates of the Cd and S precursors was essential to achieve this level of homogeneity in the core/crown dimensions and turn the reaction mixture into a purified dispersion of core/crown NPLs with long term colloidal stability and a PLQY of 92%. The average core and core/crown dimensions have been used to represent

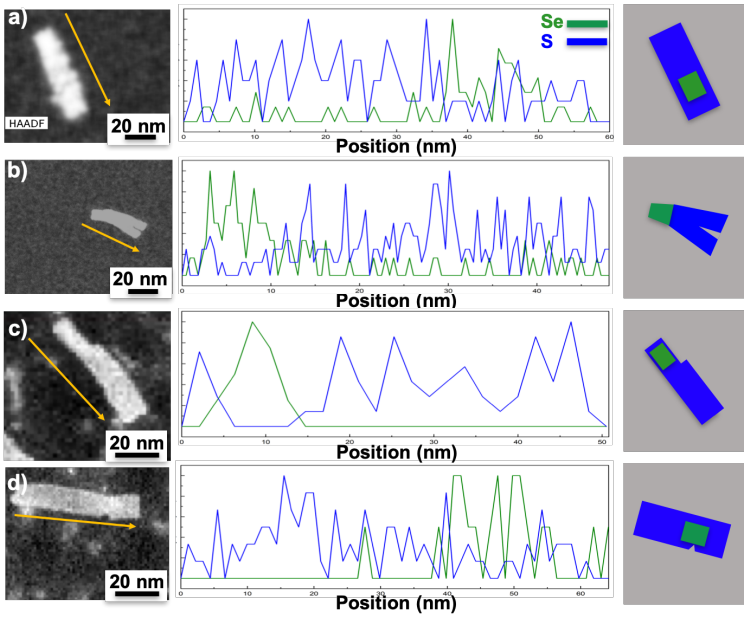

Figure 2: STEM-EDX shows the distribution of Se and S in different NPLs. From left to right are depicted a HAADF image of the analysed NPL, the corresponding extracted EDX line-profile along that NPL and a schematic of its 2D morphology and the chalcogenide distribution. In the individual horizontal panels we depict: a) A rectangular NPL corresponding to the majority of the analysed NPLs where Se is embedded by S on both sides, b) a defect riddled core/crown structure with uneven S encapsulation and a large indent, c) a NPL with uneven width and d) a NPL with an indent in the crown at the height of the core CdSe.

the morphology of an average core/crown NPL to scale in Figure 1b. Note that this average representation is most likely an idealized picture that may conceal a wide variety of side and edge thicknesses of the CdS crown.

To investigate the homogeneity of the core/crown morphology across an ensemble of NPLs, we imaged different NPLs using high angle annular dark field scanning STEM (HAADF-STEM), while simultaneously analyzing the local composition by energy dispersive x-ray spectroscopy (EDX). Due to the presence of residual ligands around the NPLs and the sensitivity of the NPLs to the electron beam, we restricted this STEM-EDX mapping to line profiles of Se and S along the long axis of a given NPL. In this way, a reasonable signal-to-noise ratio could be obtained despite the carbon contamination, whilst also avoiding sample damage. Out of a set of 19 NPLs, we found that 17 NPLs exhibited a CdS crown on both sides of the CdSe core, suggesting a complete lateral encapsulation of the core by the crown.

A representative example of this NPL subset is shown in Figure 2a. Here, the line profile of S extends along the full NPL length, whereas the Se signal is restricted to a region that covers only part of the NPL. Note that the core Se is found closer to one of the NPL edges rather than in the NPL center and that the S signal does not vanish when the core is imaged. In line with the HAADF-STEM image of this NPL, such a line scan suggests a morphology as shown in Figure 2a, where an off-center CdSe core is embedded within a rectangular CdS crown. Figure 2b provides an example of a NPL not following this dominant picture. In this case, S is only detected at one side of the core Se, which indicates the formation of a partial crown. Furthermore, the STEM image even shows a split top surface on the other end of this NPL. Next to the completeness of the CdS crown, the HAADF-STEM images also enabled us to evaluate smaller deviations from the ideal core/crown morphology as depicted in Figure 1b. Figure 2c, for example, shows a NPL for which the combination of the STEM-EDX map and the HAADF-STEM image suggests a morphology in which a narrow, CdSe-rich side is combined by a wider, one-sided CdS crown. The NPL depicted in Figure 2d, on the other hand, features an indent at the height of the CdSe core, possibly exposing the CdSe edge to the surroundings. Additional examples of NPLs featuring crowns such minor defects, such as bends and indents, are given in Supporting Information S2. Based on this TEM analysis, we conclude that the core/crown synthesis leads on average to the formation of a sizeable CdS crown on each CdSe edge. However, notwithstanding this average core/crown morphology, it appears that an entire ensemble still contains a significant fraction of defective core/crown NPLs with partially exposed CdSe edges.

We analyzed the surface chemistry of CdSe/CdS core/crown NPLs by means of solution ^{1}H nuclear magnetic resonance (NMR) spectroscopy, a most powerful approach to study ligand binding and ligand exchange reactions for colloidal nanocrystals.[39] Figure 3a depicts the ^{1}H spectrum of a purified dispersion of core/crown NPLs in cyclohexane-d_{12}. Similar to the case of CdSe NPLs,[35] the spectrum features the characteristic resonances of bound oleate moieties, for which well-resolved resonances are retrieved on top of a broad pedestal.

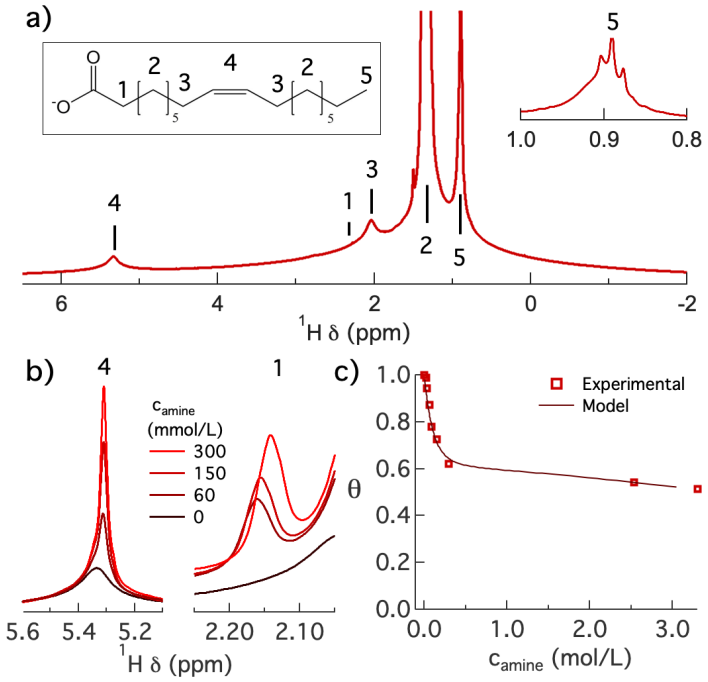

Figure 3: (a) ^{1}H-NMR spectrum of a well-purified dispersion of core/crown CdSe/CdS NPLs. The proton resonances are annotated according to the numbering on the oleate moiety depicted. Inset: zoom on the methyl resonance **1** used in parallel with the alkene resonance to quantify the total ligand concentration. (b) Overlay of the ^{1}H-NMR spectra recorded at different steps during the amine titration around (left) the alkene resonance **4** and (right) the $\alpha - CH_2$ resonance **1**. In both cases, sharper resonances develop, an evolution indicative of $Cd(Ol)_2$ displacement. (c) The displacement isotherm of $Cd(Ol)_2$ depicting the bound fraction θ as a function of the concentration of $BuNH_2$ added. The markers indicated data retrieved from NMR spectra, whereas the line represents a simulated isotherm based on the two-site binding model with parameters K_1, K_2 and α as summarized in Table 1.

In line with existing literature, the resonances in Figure 3a were assigned to the different oleate protons as indicated in the inset of Figure 3a.[40] Note that these resonances are all broadened and shifted relative to the resonances of neat oleic acid in cyclohexane, a typical characteristic of surface bound ligands.[39] Integrating the CH_3 resonances **5** at 0.92 ppm and the alkene proton resonance **4** at 5.37 ppm yields an integrated intensity ratio I_5/I_4 of 1.63. Being close to the expected 3:2 ratio of both resonance intensities for oleic acid, we can conclude that the synthesis and purification protocol implemented here results in nearly exclusively oleate capped NPLs, despite the use of cadmium octanoate during the synthesis.

The oleate moieties found on the surface of core/crown NPLs are introduced as cadmium

oleate in the final step of the synthesis. In accordance with literature studies on CdSe QDs and CdSe NPLs,[35,40] we therefore assume that the actual ligand binding to the core/crown NPL surface is best seen as cadmium oleate ($Cd(Ol)_2$). It is well-known that such so-called Z-type ligands or Lewis acids can be stripped from a metal chalcogenide surface by addition of L-type ligands or Lewis bases, such as aliphatic primary amines.[37] By adding butylamine ($BuNH_2$) to a dispersion of CdSe NCs, this L-type driven Z-type stripping has been used to probe the $Cd(Ol)_2$ binding sites by means of the following equilibrium reaction where amines coordinate the desorbing $Cd(Ol)_2$ complex and leave behind an empty surface site:[38]

$$[CdSe](Cd(Ol)_2) + 2BuNH_2 \rightleftharpoons [CdSe](\circ) + Cd(Ol)_2 - (BuNH_2)_2 \quad (1)$$

Here, [CdSe] refers to the stoichiometric CdSe NCs, ($Cd(Ol)_2$) is a surface-bound cadmium oleate and ($\circ$) is an empty surface site. Note that the displacement equilibrium as expressed by Eq. 1 neglects the back adsorption of $BuNH_2$.[38]

Here, we used a $BuNH_2$ titration to quantify the binding of $Cd(Ol)_2$ to the surface of CdSe/CdS core/crown NPLs. Figure 3b illustrates the evolution of the $\alpha - CH_2$ resonance **1** and the alkene resonance **4** of $Cd(Ol)_2$ during such a titration. In both cases, the appearance of a more narrow resonance is indicative of the formation of desorbed oleate moieties, where in particular the narrow $\alpha - CH_2$ resonance **1** enables the concentration of desorbed cadmium oleate to be quantified.[35] We confirmed the co-removal of Cd during ligand stripping by elemental analysis of the supernatant, in which only Cd and no Se is detected by x-ray fluorescence after ligand stripping, see Supporting Information S2. The resulting isotherm from the titration, showing the relative surface coverage θ of cadmium oleate at each step, is represented in Figure 3c. A detailed account of the spectra and fitting procedures underlying the isotherm determination is provided in Supporting Information S3. We retrieve a surface coverage that quickly drops in the initial stage of the titration between a $BuNH_2$ concentration of 0 and 0.3 mol/L; the latter concentration corresponding to a $BuNH_2$: $Cd(Ol)_2$

Table 1: Parameters of the two site binding model for CdSe NPLs as reported by Singh et al.[35] and CdSe/CdS core/crown NPLs investigated here.

	K_1	K_2	α
CdSe NPLs	3.0	$2\,10^{-3}$	0.375
CdSe/CdS NPLs	0.3	$7\,10^{-5}$	0.400

equivalence of 20. At higher $BuNH_2$ concentrations, the relative surface coverage of $Cd(Ol)_2$ is largely constant, at about 60% of the initial surface coverage. In line with previous studies on CdSe nanocrystals and CdSe NPLs, we assign these two regimes to binding site heterogeneity,[35,38] where loosely bound ligands are displaced in the initial stage of the titration, while strongly bound ligands remain on the NPL surface also at high $BuNH_2$ concentrations.

Following the idea of binding site heterogeneity, we described the adsorption isotherm by means of a two-site binding model that distinguishes weak binding sites **1** from strong binding sites **2**:

$$[CdX](Cd(Ol)_2)_1 + 2BuNH_2 \rightleftharpoons [CdX](\circ)_1 + Cd(Ol)_2 - (BuNH_2)_2 \quad (2)$$

$$[CdX](Cd(Ol)_2)_2 + 2BuNH_2 \rightleftharpoons [CdX](\circ)_2 + Cd(Ol)_2 - (BuNH_2)_2 \quad (3)$$

Describing the underlying nanocrystal as CdX highlights that we do not distinguish at this stage of the analysis between cadmium oleate binding to undercoordinated S or Se at the core/crown surface; we will come back to this point later. Translating the set of coupled equilibrium equations into an expression for the relative surface coverage as a function of the $BuNH_2$ concentration, see Supporting Information S3, we can simulate the measured isotherms taking the respective equilibrium constants K_1 and K_2 and the fraction α of weak binding sites as adjustable parameters. The full line in Figure 3c represents the result of such a simulation, which was obtained by taking K_1, K_2 and α as summarized in Table 1. Similar to CdSe QDs and NPLs, Figure 3c shows that the 2-site model describes the main features of the adsorption isotherm, in this case by taking $K_1 = 0.3$, $K_2 = 7.0\,10^{-5}$, and $\alpha = 0.4$.

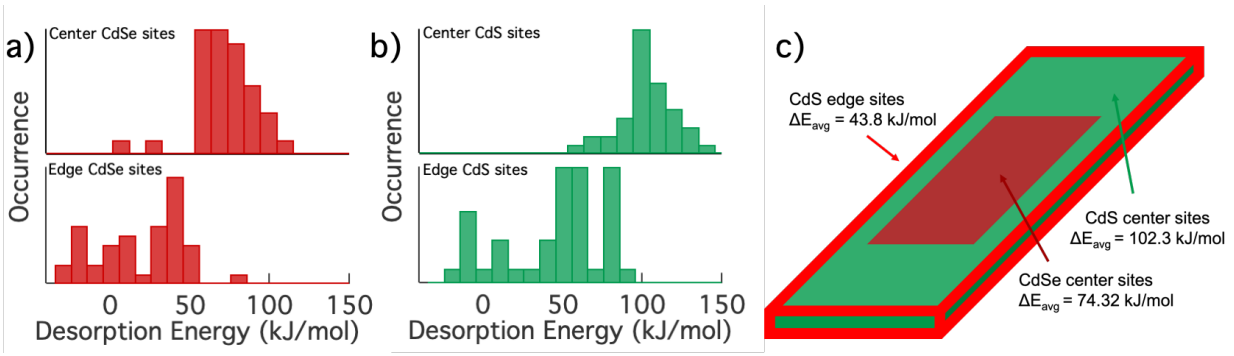

Figure 4: (a) Histograms representing the desorption energy in kJ/mol for the displacement of $CdCl_2$ from a model CdSe NPL by complexation with $BuNH_2$ from (top) (near)-edge sites and (bottom) facet sites. (b) The same for displacement from a model CdS NPL. (c) Schematic representation of the average desorption energies for the relevant binding sites of a CdSe/CdS core/crown NPL.

To evaluate the fraction of weak binding sites **1**, we start from the consideration that CdSe/CdS core/crown NPLs have an average morphology as outlined in Figure 1b. Assuming the edges are homogeneous, we can then partition the total surface area into edge or vertex sites and facet sites. In agreement with CdSe NPLs, we identify the former with all sites localized within 2 lattice planes of an edge. Given the core/crown dimensions, this approach predicts that 34% of the binding sites of a core/crown NPL are edge sites and 66% facet sites, see Supporting Information S3. Such an edge-site fraction closely agrees with the fraction α=0.40 of weak binding sites **1** retrieved from the two-site binding model. Possibly, the difference is related to the observed deviations from the presumed rectangular shape, which will all enhance the fraction of (near)-edge sites. Even so, the agreement supports the tentative conclusion that in the first stage of the isotherm, $BuNH_2$ displaces cadmium oleate near the edges of the core/crown NPLs. In that case, the significantly lower equilibrium constant K_1 for the binding sites **1** of CdSe/CdS core/crown NPLs as compared to CdSe core NPLs (see Table 1) would mean that cadmium oleate binds more strongly to the CdS crown edge than to the CdSe edge of core-only NPLs.

To validate the consistency of the interpretation that $BuNH_2$ initially displaces cadmium oleate from the CdS edge, which features binding sites with a higher binding energy than

CdSe edges, we calculated the desorption energies of cadmium oleate from CdSe and CdS model NPLs using density functional theory (DFT). For computational advantage, we replaced cadmium oleate by cadmium chloride as indicated in Equation 4 and compared the total energy of the system before and after displacement:

$$[\mathrm{CdS}](\mathrm{Cd(Cl)_2}) + 2\mathrm{BuNH_2} \rightleftharpoons [\mathrm{CdS}](\circ) + \mathrm{Cd(Cl)_2} - (\mathrm{BuNH_2})_2 \tag{4}$$

Note that after ligand displacement, we allowed for the full structural relaxation of the remaining NPL before calculating the displacement energy. Figure 4 represents the thus obtained desorption energy for sites across CdSe and CdS NPLs in terms of histograms for the centrally located sites and near-edge sites. While the results for CdSe NPLs are identical to what was published previously, we indeed find that CdS NPLs systematically show larger displacement energies than CdSe NPLs. Moreover, the center of the facets feature largely site-independent displacement energies as can be seen by the narrow distribution of desorption energies, whereas the first and second row of binding sites near the edge exhibit a broader range of displacement energies. The desorption energies per surface site are represented in Supporting Information **??**. Importantly, with an average displacement energy of 43.8 kJ/mol, the CdS edge sites are significantly weaker than the facet sites of CdS (102.3 kJ/mol) and CdSe (74.3 kJ/mol) NPLs (see Figure 4c). Hence, we conclude that for the average core/crown NPL, the weaker binding sites **1** effectively correspond to the CdS edge sites.

In Figure 5, we present photoluminescence (PL) spectra of two dispersions of core/crown NPLs during a titration with $BuNH_2$, where intensities were normalized relative to the initial, purified dispersion. For these measurements, we used an excitation wavelength of 460 nm to ensure that excitons are exclusively formed within the CdSe core. In the case of an unoptimized core/crown NPLs sample, in which most NPLs have an incomplete crown (see Supporting Information S2), the addition of small amounts of $BuNH_2$ leads to a rapid

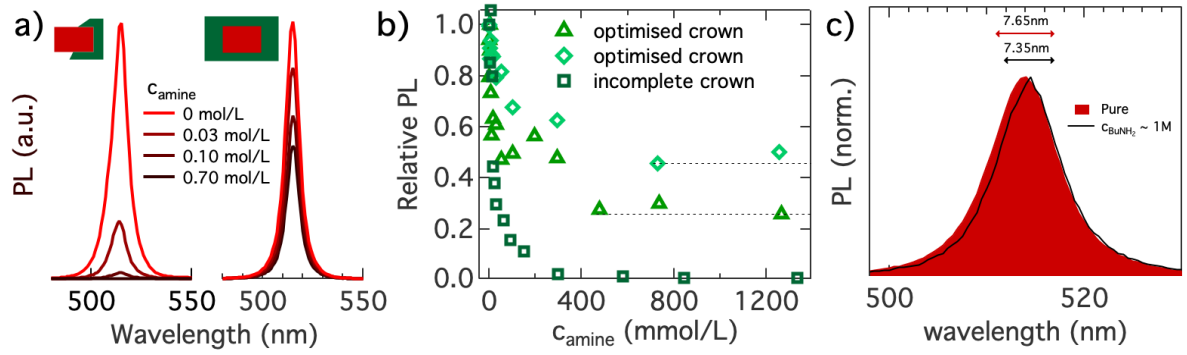

Figure 5: (a) Photoluminescence spectra of CdSe/CdS core/crown NPLs at different steps during a $BuNH_2$ titration including (left) incomplete core/crown and (right) optimised core/crown NPLs. For both samples, PL spectra have been normalized relative to the initial spectrum, i.e., before $BuNH_2$ addition. (b) Evolution of the relative PLQY during $BuNH_2$ titration for (squares) NPLs with an incomplete crown and (diamonds, triangles) two different samples synthesized following the optimized procedure. (c) PL spectrum of CdSe/CdS core/crown NPLs recorded before $BuNH_2$ addition and for a $BuNH_2$ concentration of 1 M, *i.e.*, well inside the displacement plateau.

loss of the PL. Complete quenching is attained at a $BuNH_2$ concentration of 0.4 M, which corresponds to the onset of the isotherm plateau. Interestingly, this evolution of the PL closely agrees with the loss of PL upon $BuNH_2$ addition to core CdSe NPLs.[35] On the other hand, upon addition of $BuNH_2$ to CdSe/CdS core/crown dispersions synthesized with the optimized procedure, the initial rapid drop of the PL efficiency gives way to a plateau where the PLQY levels off at a sample-dependent level of 30% or even 45% of the initial value. As shown in Figure 5, the photoluminescence spectrum under these conditions remains characteristic of CdSe exciton recombination. Moreover, comparing normalized spectra before the titration and well within the titration plateau, one sees that the emission line is slightly more narrow and red shifted after $BuNH_2$ addition; an evolution that reflects a preferential quenching of the blue side of the emission line.

The loss of PLQY upon $BuNH_2$ addition can either reflect a gradual reduction of the emission efficiency for each NPL, or the progressive formation of a dark fraction within the ensemble. In order to distinguish both possibilities, Figure 6 represents the results of a time-resolved photoluminescence study on a CdSe/CdS core/crown sample synthesized using the

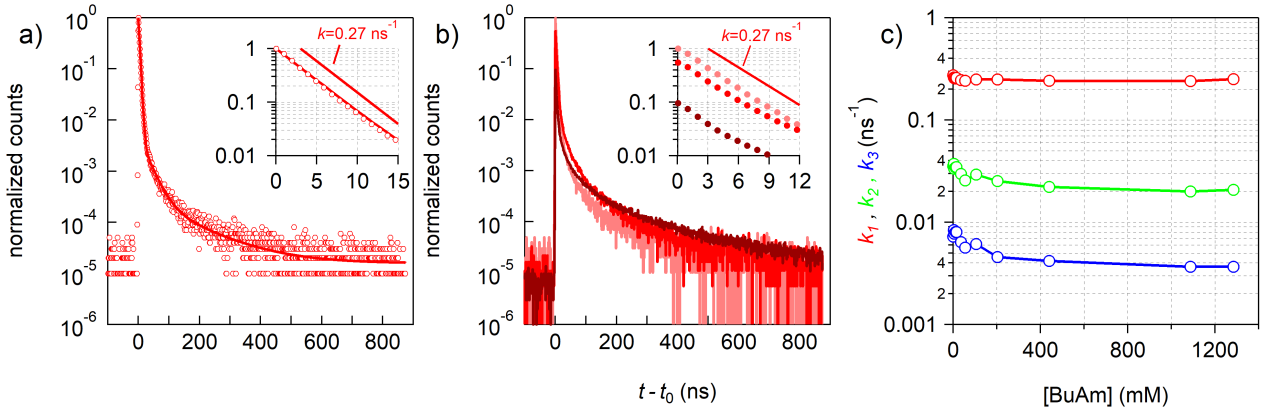

Figure 6: (a) Transient photoluminescence recorded on the initial core/crown sample, including (markers) measured data and (full line) 3-exponential fit. (inset) Zoom on the first 15 ns of the decay. The reference line represents a single exponential decay with an emission rate of 0.27 ns^{-1}. (b) Transient photoluminescence of the (light red) initial sample, (red) after addition of 55 mM of $BuNH_2$ and (dark red) 1285 mM of $BuNH_2$. The traces have been normalized such that the integrated intensity is proportional to the PLQY of the respective samples. (inset) Zoom on the first 15 ns of the decay. The reference line represents a single exponential decay with an emission rate of 0.27ns^{-1}. (c) Different rate constants obtained by fitting a 3-exponential decay to the transient photoluminescence as a function of the $BuNH_2$ concentration.

optimized procedure. Here, all samples were excited by pulsed excitation with a 0.5 MHz repetition rate at 460 nm. As a starting point, Figure 6a displays the PL decay of the initial sample, which had a 90% PLQY. We find that the intensity transient $I(t)$ is dominated by a single exponential decay component that gives way to a minor tail of delayed emission. As can be seen in the inset of Figure 6a, the decay rate k_1 of the dominant component amounts to 0.27 ns^{-1}, a typical number for radiative exciton recombination in NPLs.[41] Starting from this assignment, we attribute the delayed emission to carrier capture-and-release processes that slow down exciton recombination without inducing additional emission bands in the PL spectrum. In Figure 6b, we reproduce the original PL transient in combination with two transients recorded after addition of 55 mM and 1285 mM of $BuNH_2$; concentrations that correspond to the region of the initial PL drop and the PL plateau, respectively. Here, all transients have been scaled such that the integrated intensity is proportional to the PLQY of the sample. For the three transients, we observe the same initial single-exponential decay

followed by a tail of delayed emission that exhibits, by-and-large, the same decay profile.

Given this similar time-dependence, we analyzed all decay traces in more detail by a fit to the same sum of three exponentials and a constant background component matched to the remaining signal intensity prior to excitation:

$$I(t) = A_0 + A_1 e^{-k_1 t} + A_2 e^{-k_2 t} + A_3 e^{-k_3 t} \tag{5}$$

For the initial PL decay, the fit result has been added to Figure 6a. For all other samples, the recorded decay traces and the fits can be found in Supporting Information S3. Figure 6c represents the thus obtained rate constants. In line with the initial observation, we find that the rate of the fastest component (k_1), which we assigned to direct radiative exciton recombination, is independent of the $BuNH_2$ concentration while the rate of the slower components drops by no more than a factor of 2. Importantly, none of these rate constants speeds up, which suggests that for the NPLs that keep emitting throughout the titration, competition with non-radiative decay components remains absent. More quantitatively, the combination of amplitudes and rates obtained through the fit indicates that for the initial sample, 95% of the emitted photons are contained in the direct radiative exciton component. For samples in the PL plateau, this fraction is still at 64%, see Supporting Information S3. Hence, direct radiative exciton recombination remains the dominant emission component for the remaining emitting NPLs during a $BuNH_2$ titration. Accordingly, we conclude that $BuNH_2$ titration splits the NPL population in two fractions. For the first fraction, ligand stripping leads to the complete quenching of the PL, a process that accounts for the observed PL efficiency drop. For the second fraction, on the other hand, $BuNH_2$ addition only leads to minor changes in the PL dynamics without affecting, most importantly, the radiative recombination rate.

Bringing together the results of the structural characterization, the evolution of the surface chemistry, the steady-state and the time-resolved photoluminescence during $BuNH_2$

titration, and the theoretical analysis of the $Cd(Ol)_2$ binding energy leads to a consistent picture of the relation between surface chemistry and opto-electronic properties of CdSe core and CdSe/CdS core/crown NPLs. For both systems, the combination of $Cd(Ol)_2$ displacement and the theoretical estimates of the $Cd(Ol)_2$ binding energy leads to the conclusion that ligands are preferentially stripped from (near)-edge binding sites, which induce mid-gap states that quench the photoluminescence in the case of CdSe NPLs. Importantly, CdSe/CdS core/crown NPLs have a straddling band alignment that keeps the exciton localized within the CdSe core;[28] a point well exemplified by the absorption and photoluminescence spectra shown in Figure 1 which feature separate CdSe and CdS exciton lines in absorption yet only CdSe exciton emission. Under such conditions, ligand stripping from the CdS edge of core/crown NPLs should not affect the radiative exciton recombination given that a fully homogeneous crown is grown around the CdSe core. The comparison of PL quenching upon $BuNH_2$ addition to defective and optimized core/crown NPLs indicates that this is indeed the case. Defective NPLs exhibit a loss of photoluminescence comparable to CdSe core NPLs, indicating that indeed part of the CdSe edge remains unpassivated. On the other hand, optimized core/crown NPLs preserve a significant fraction of the original PL efficiency; a result we assign to the combined presence of NPLs with a defective and a homogeneous CdS crown as confirmed by the STEM-HAADF imaging shown in Figure 2. The identification of well and poorly crowned NPLs in an ensemble is further confirmed by transient photoluminescence during ligand stripping, which also gave evidence of two populations. At this point, the identification of the emitting fraction – for which the radiative recombination rate of the excitons remains unchanged – with perfectly crowned NPLs and the dark fraction with imperfectly crowned NPLs becomes straightforward. Interestingly, the preferential loss of the blue side of the exciton emission supports this conclusion. Since crown growth shifts the exciton emission to longer wavelengths, NPLs with incomplete crowns will, on average, experience less of a red shift.

Importantly, the link between ligand stripping and photoluminescence quenching in core

and core/crown NPLs highlights that (100) facets passivated by Z-type ligands such as $Cd(Ol)_2$ lead to nanocrystals with clean HOMO-LUMO gaps, *i.e.*, without localized mid-gap states. Moreover, Z-type ligand binding to such a facet is strong and withstands the relatively harsh ligand stripping environment created by $BuNH_2$ addition. This conclusion explains why CdSe core and CdSe/CdS core/crown NPLs can be grown with a PLQY of 50 to nearly 100% without full passivation by an inorganic shell, which has been since long the main paradigm to form colloidal semiconductor NCs with an efficient band-edge photoluminescence. Opposite from the binding sites on the (100) facet, we find that (near)-edge binding sites are weaker and more vulnerable to ligand displacement. In the case of 2D NPLs, such sites are well-localized on the NPL surface and edge passivation by the mere growth of a CdS crown suffices to turn CdSe NPLs into more robust CdSe/CdS core/crown structures. For spherical NCs, on the other hand, edge sites are plenty and distributed over the entire NC surface. As a result, homogeneous shelling is typically the most staightforward surface passivation approach. Even if the saturation of the surface with Z-type ligands can suffice to attain nearly 100% PLQY, our work suggests that such NCs remain prone to photoluminescence quenching since the ubiquitous edge sites will bind Z-type ligands more weakly.

In summary, this work addresses the interrelation between surface chemistry and opto-electronic properties in colloidal semiconductor nanocrystals using core/crown CdSe/CdS NPLs as a model system. The NPLs have an atomically precise thicknesses and feature $Cd(Ol)_2$ covered (100) facets. Purified core/crown NPLs can have a photoluminescence quantum yield exceeding 90%. Even so, STEM images indicate that NPLs can have defective crowns. We show that addition of $BuNH_2$ to such a NPL dispersion induces the displacement of $Cd(Ol)_2$ from the NPL surface in conjunction with a drop of the PLQY. However, opposite from CdSe NPLs, a displacement plateau is reached in which a NPL dispersion can retain up to 45% of its initial PLQY. Moreover, we find that during a $BuNH_2$, direct radiative exciton recombination remains the dominant component in the PL transient.

Building on simulations of the $CdCl_2$ binding energy to CdSe and CdS model NPLs, we infer that these observations reflect the preferential stripping of $Cd(Ol)_2$ from (near)-edge sites. Given the localization of the exciton in the CdSe core, such a process will leave the fraction of CdSe/CdS core/crown NPLs with a complete CdS crown untouched. Hence, we conclude that passivation of edge sites is key to form semiconductor nanocrystals with an efficient and robust photoluminescence.

Acknowledgement

Z.H. and S.B. acknowledge support by SIM-Flanders (SBO-QDOCCO). Z.H. acknowledges support by FWO-Vlaanderen (research project 17006602). Z.H. and I.M. acknowledge support by Ghent University (GOA n° 01G01019). J.L. acknowledges FWO-vlaanderen for a fellowship (SB PhD fellow at FWO). Sh.S acknowledges FWO postdoctoral funding (FWO17/PDO/184). This project has further received funding from the European Research Counsil under the European Union's Horizon 2020 research and innovation programme (ERC Consolidator grant no. 815128 REALNANO and starting grant no. 714876 PHOCONA).

Supporting Information Available

The Supporting Information is available free of charge via the Internet at http://pubs.acs.org/.

Full experimental details concerning the synthesis as well as the titration experiments can be retrieved in the supporting information alongside the fitting of the NMR data, derivation of the two site model as well as calculation of the weakly bound fraction of ligands according to the geometry of the NPL.

References

(1) Talapin, D. V.; Lee, J.-S.; Kovalenko, M. V.; Shevchenko, E. V. Prospects of Colloidal Nanocrystals for Electronic and Optoelectronic Applications. *Chem. Rev.* **2009**, *110*, 389–458.

(2) Kovalenko, M. V.; Manna, L.; Cabot, A.; Hens, Z.; Talapin, D. V.; Kagan, C. R.; Klimov, V. I.; Rogach, A. L.; Reiss, P.; Milliron, D. J. et al. Prospects of Nanoscience with Nanocrystals. *ACS Nano* **2015**, *9*, 1012–1057.

(3) Kagan, C. R.; Lifshitz, E.; Sargent, E. H.; Talapin, D. V. Building Devices from Colloidal Quantum Dots. *Science* **2016**, *353*, aac5523.

(4) Bourzac, K. Quantum dots go on display. *Nature* **2013**, *493*, 283–283.

(5) Wood, V.; Bulović, V. Colloidal Quantum Dot Light-Emitting Devices. *Nano Rev.* **2010**, *1*, 5202.

(6) Moon, H.; Lee, C.; Lee, W.; Kim, J.; Chae, H. Stability of Quantum Dots, Quantum Dot Films, and Quantum Dot Light-Emitting Diodes for Display Applications. *Adv. Mater.* **2019**, 1804294.

(7) Hines, D. A.; Kamat, P. V. Recent Advances in Quantum Dot Surface Chemistry. *ACS Appl. Mater. Interfaces* **2014**, *6*, 3041–3057.

(8) Yu, M.; Fernando, G.; Li, R.; Papadimitrakopoulos, F.; Shi, N.; Ramprasad, R. First Principles Study of CdSe Quantum Dots: Stability, Surface Unsaturations, and Experimental Validation. *Appl. Phys. Lett.* **2006**, *88*, 231910.

(9) Knowles, K. E.; Frederick, M. T.; Tice, D. B.; Morris-Cohen, A. J.; Weiss, E. A. Colloidal Quantum Dots: Think Outside the (Particle-in-a-)Box. *J. Phys. Chem. Lett.* **2011**, *3*, 18–26.

(10) Kirkwood, N.; Monchen, J. O.; Crisp, R. W.; Grimaldi, G.; Bergstein, H. A.; du Fossé, I.; van der Stam, W.; Infante, I.; Houtepen, A. J. Finding and Fixing Traps in II–VI and III–V Colloidal Quantum Dots: The Importance of Z-Type Ligand Passivation. *J. Am. Chem. Soc.* **2018**, *140*, 15712–15723.

(11) Pan, J.; Shang, Y.; Yin, J.; De Bastiani, M.; Peng, W.; Dursun, I.; Sinatra, L.; El-Zohry, A. M.; Hedhili, M. N.; Emwas, A.-H. et al. Bidentate Ligand-Passivated CsPbI3 Perovskite Nanocrystals for Stable Near-Unity Photoluminescence Quantum Yield and Efficient Red Light-Emitting Diodes. *J. Am. Chem. Soc.* **2018**, *140*, 562–565, PMID: 29249159.

(12) Munro, A. M.; Jen-La Plante, I.; Ng, M. S.; Ginger, D. S. Quantitative Study of the Effects of Surface Ligand Concentration on CdSe Nanocrystal Photoluminescence. *J. Phys. Chem. C* **2007**, *111*, 6220–6227.

(13) Bullen, C.; Mulvaney, P. The Effects of Chemisorption on the Luminescence of CdSe Quantum Dots. *Langmuir* **2006**, *22*, 3007–3013.

(14) Dabbousi, B. O.; Rodriguez-Viejo, J.; Mikulec, F. V.; Heine, J. R.; Mattoussi, H.; Ober, R.; Jensen, K. F.; Bawendi, M. G. (CdSe)ZnS Core-Shell Quantum Dots: Synthesis and Characterization of a Size Series of Highly Luminescent Nanocrystallites. *J. Phys. Chem. B* **1997**, *101*, 9463–9475.

(15) Talapin, D. V.; Rogach, A. L.; Kornowski, A.; Haase, M.; Weller, H. Highly Luminescent Monodisperse CdSe and CdSe/ZnS Nanocrystals Synthesized in a Hexadecylamine-Trioctylphosphine Oxide-Trioctylphosphine Mixture. *Nano Lett.* **2001**, *1*, 207–211.

(16) Haubold, S.; Haase, M.; Kornowski, A.; Weller, H. Strongly Luminescent InP/ZnS Core–Shell Nanoparticles. *ChemPhysChem* **2001**, *2*, 331–334.

(17) Peng, X.; Schlamp, M. C.; Kadavanich, A. V.; Alivisatos, A. P. Epitaxial Growth

of Highly Luminescent CdSe/CdS Core/Shell Nanocrystals with Photostability and Electronic Accessibility. *J. Am. Chem. Soc.* **1997**, *119*, 7019–7029.

(18) Houtepen, A. J.; Hens, Z.; Owen, J. S.; Infante, I. On the Origin of Surface Traps in Colloidal II–VI Semiconductor Nanocrystals. *Chem. Mater.* **2017**, *29*, 752–761.

(19) Giansante, C.; Infante, I. Surface Traps in Colloidal Quantum Dots: A Combined Experimental and Theoretical Perspective. *J. Phys. Chem. Lett.* **2017**, *8*, 5209–5215.

(20) Stein, J. L.; Mader, E. A.; Cossairt, B. M. Luminescent InP Quantum Dots with Tunable Emission by Post-Synthetic Modification with Lewis Acids. *J. Phys. Chem. Lett.* **2016**, *7*, 1315–1320.

(21) Joo, J.; Son, J. S.; Kwon, S. G.; Yu, J. H.; Hyeon, T. Low-Temperature Solution-Phase Synthesis of Quantum Well Structured CdSe Nanoribbons. *J. Am. Chem. Soc.* **2006**, *128*, 5632–5633.

(22) Son, J. S.; Park, K.; Kwon, S. G.; Yang, J.; Choi, M. K.; Kim, J.; Yu, J. H.; Joo, J.; Hyeon, T. Dimension-Controlled Synthesis of CdS Nanocrystals: From 0D Quantum Dots to 2D Nanoplates. *Small* **2012**, *8*, 2394–2402.

(23) Son, J. S.; Yu, J. H.; Kwon, S. G.; Lee, J.; Joo, J.; Hyeon, T. Colloidal Synthesis of Ultrathin Two-Dimensional Semiconductor Nanocrystals. *Adv. Mater.* **2011**, *23*, 3214–3219.

(24) Ithurria, S.; Dubertret, B. Quasi 2D Colloidal CdSe Platelets with Thicknesses Controlled at the Atomic Level. *J. Am. Chem. Soc.* **2008**, *130*, 16504–16505.

(25) Ithurria, S.; Tessier, M.; Mahler, B.; Lobo, R.; Dubertret, B.; Efros, A. L. Colloidal Nanoplatelets with Two-Dimensional Electronic Structure. *Nat. Mater.* **2011**, *10*, 936.

(26) Gerdes, F.; Navío, C.; Juárez, B. H.; Klinke, C. Size, Shape, and Phase Control in Ultrathin CdSe Nanosheets. *Nano Lett.* **2017**, *17*, 4165–4171.

(27) Christodoulou, S.; Climente, J. I.; Planelles, J.; Brescia, R.; Prato, M.; Martín-García, B.; Khan, A. H.; Moreels, I. Chloride-Induced Thickness Control in CdSe Nanoplatelets. *Nano Lett.* **2018**, *18*, 6248–6254.

(28) Tessier, M. D.; Javaux, C.; Maksimovic, I.; Loriette, V.; Dubertret, B. Spectroscopy of Single CdSe Nanoplatelets. *ACS Nano* **2012**, *6*, 6751–6758.

(29) Mahler, B.; Nadal, B.; Bouet, C.; Patriarche, G.; Dubertret, B. Core/Shell Colloidal Semiconductor Nanoplatelets. *J. Am. Chem. Soc.* **2012**, *134*, 18591–18598.

(30) Polovitsyn, A.; Dang, Z.; Movilla, J. L.; Martín-García, B.; Khan, A. H.; Bertrand, G. H.; Brescia, R.; Moreels, I. Synthesis of Air-Stable CdSe/ZnS Core–Shell Nanoplatelets with Tunable Emission Wavelength. *Chem. Mater.* **2017**, *29*, 5671–5680.

(31) Sun, H.; Buhro, W. E. Core-Shell Cadmium Telluride Quantum Platelets with Absorptions Spanning the Visible Spectrum. *ACS Nano* **2019**, *13*, 6982–6991.

(32) Rossinelli, A. A.; Riedinger, A.; Marqués-Gallego, P.; Knüsel, P. N.; Antolinez, F. V.; Norris, D. J. High-temperature Growth of Thick-Shell CdSe/CdS Core/Shell Nanoplatelets. *Chem. Commun.* **2017**, *53*, 9938–9941.

(33) Tessier, M. D.; Spinicelli, P.; Dupont, D.; Patriarche, G.; Ithurria, S.; Dubertret, B. Efficient Exciton Concentrators Built from Colloidal Core/Crown CdSe/CdS Semiconductor Nanoplatelets. *Nano Lett.* **2013**, *14*, 207–213.

(34) Prudnikau, A.; Chuvilin, A.; Artemyev, M. CdSe–CdS Nanoheteroplatelets with Efficient Photoexcitation of Central CdSe Region through Epitaxially Grown CdS Wings. *J. Am. Chem. Soc.* **2013**, *135*, 14476–14479.

(35) Singh, S.; Tomar, R.; Ten Brinck, S.; De Roo, J.; Geiregat, P.; Martins, J. C.; Infante, I.; Hens, Z. Colloidal CdSe Nanoplatelets, A Model for Surface Chemistry/Optoelectronic

Property Relations in Semiconductor Nanocrystals. *J. Am. Chem. Soc.* **2018**, *140*, 13292–13300.

(36) Lhuillier, E.; Pedetti, S.; Ithurria, S.; Nadal, B.; Heuclin, H.; Dubertret, B. Two-Dimensional Colloidal Metal Chalcogenides Semiconductors: Synthesis, Spectroscopy, and Applications. *Acc. Chem. Res.* **2015**, *48*, 22–30.

(37) Anderson, N. C.; Hendricks, M. P.; Choi, J. J.; Owen, J. S. Ligand Exchange and the Stoichiometry of Metal Chalcogenide Nanocrystals: Spectroscopic Observation of Facile Metal-Carboxylate Displacement and Binding. *J. Am. Chem. Soc.* **2013**, *135*, 18536–18548.

(38) Drijvers, E.; De Roo, J.; Martins, J. C.; Infante, I.; Hens, Z. Ligand Displacement Exposes Binding Site Heterogeneity on CdSe Nanocrystal Surfaces. *Chem. Mater.* **2018**, *30*, 1178–1186.

(39) Hens, Z.; Martins, J. C. A Solution NMR Toolbox for Characterizing the Surface Chemistry of Colloidal Nanocrystals. *Chem. Mater.* **2013**, *25*, 1211–1221.

(40) Fritzinger, B.; Capek, R. K.; Lambert, K.; Martins, J. C.; Hens, Z. Utilizing Self-Exchange To Address the Binding of Carboxylic Acid Ligands to CdSe Quantum Dots. *J. Am. Chem. Soc.* **2010**, *132*, 10195–10201.

(41) Kunneman, L. T.; Schins, J. M.; Pedetti, S.; Heuclin, H.; Grozema, F. C.; Houtepen, A. J.; Dubertret, B.; Siebbeles, L. D. Nature and Decay Pathways of Photoexcited States in CdSe and CdSe/CdS Nanoplatelets. *Nano Lett.* **2014**, *14*, 7039–7045.